



Internal geophysics (Geodesy)

Use of Starlette and LAGEOS-1&-2 laser measurements for determination and analysis of stations coordinates and EOP time series

Utilisation des mesures laser de Starlette et LAGEOS-1&-2 pour la détermination et l'analyse des séries temporelles des coordonnées de stations et des EOP

Bachir Gourine

Division de géodésie spatiale, centre des techniques spatiales (CTS), BP 13, 31200 Arzew, Algeria

ARTICLE INFO

Article history:

Received 27 February 2011

Accepted after revision 13 May 2012

Available online 23 June 2012

Presented by Jean Kovalevsky

Keywords:

Inter-satellite combination

Starlette

LAGEOS-1&-2

SLR technique

EOP

Geocenter

Frequency analysis

Noise estimation

ABSTRACT

The purpose of this article is to study the contribution of a LEO satellite (Starlette) laser measurements in the estimation of the geodetic products, such as station coordinates, Earth Orientation Parameters (EOP), and Geocenter component variations, over a 14 year period (1993–2007). Three data combinations are considered in the processing, namely LAGEOS-1 (LA-1), LAGEOS-1&-2 (LA-1&LA-2) and LAGEOS-1&Starlette (LA-1&STAR). The orbit computation of the different satellites is performed with GINS software and the laser data processing is carried out by MATLO software, with consideration of a recent GRACE gravity model (Eigen_Grace03s) in the Starlette orbit computation. The time series of results are projected according to ITRF2005, by TRANSFOR software, where the Helmert transformation parameters are obtained. A comparison of the different combinations is effectuated in terms of quality, periodic signals and noises of the weekly stations positions, EOP and Geocenter variations. The results revealed a degradation of positioning accuracy of about 3 to 5 mm when using Starlette data according to LA-1&STAR solution, but also a better capability to determine the annual and semi-annual variations of the UP coordinates and Geocenter components.

© 2012 Académie des sciences. Published by Elsevier Masson SAS. All rights reserved.

R É S U M É

Mots clés :

Combinaison Inter-satellite

Starlette

LAGEOS-1&-2

Technique SLR

EOP

Géocentre

Analyse fréquentielle

Estimation du bruit

L'objectif de cet article est l'étude de la contribution des mesures Laser d'un satellite à basse altitude nommé Starlette, dans l'estimation des produits géodésiques, tels que les coordonnées de stations, les paramètres de rotation de la Terre (EOP) et les variations des composantes du Géocentre, sur une période de 14 ans (1993–2007). Trois combinaisons de données Laser ont été considérées dans le traitement, LAGEOS-1 (LA-1), LAGEOS-1&-2 (LA-1&LA-2) et LAGEOS-1&Starlette (LA-1&STAR). Le calcul d'orbite des différents satellites est réalisé par le logiciel GINS et le traitement des mesures laser est exécuté par le logiciel MATLO, en adoptant un modèle récent du champ de gravité (Eigen_Grace-03s) pour le calcul d'orbite de Starlette. Les séries temporelles des résultats sont projetées sur le repère de référence ITRF2005, par le programme TRANSFOR, où les paramètres de transformation d'Helmert sont obtenus. Une comparaison des différentes solutions des combinaisons est effectuée suivant la qualité, les signaux périodiques et les bruits des positions hebdomadaires des stations, des EOP et des variations du Géocentre. Les résultats obtenus ont révélé une dégradation de la précision du positionnement de l'ordre de 3 à

E-mail address: bachrigourine@yahoo.com.

5 mm, en utilisant les données de Starlette suivant la solution LA-1&STAR, mais aussi une meilleure capacité à déterminer les variations annuelles et semi-annuelles des coordonnées verticales des stations (UP) et des composantes du Géocentre.

© 2012 Académie des sciences. Publié par Elsevier Masson SAS. Tous droits réservés.

1. Introduction

Satellite Laser Ranging (SLR) is one of the leading techniques of space geodesy for the establishment and maintenance of the International Terrestrial Reference Frame (ITRF), such as Very Long Baseline Interferometry (VLBI), Global Positioning System (GPS) and Doppler Orbitography Radio-positioning Integrated by Satellite (DORIS). It contributes to the frame determination by providing time series of terrestrial stations coordinates, i.e., Terrestrial Reference Frame (TRF), and Earth Orientation Parameters (EOP). Generally, for such determination, only measurements of high altitude satellites (LAGEOS-1 & LAGEOS-2, 6000 km and Etalon-1 & Etalon-2, 19000 km) are used. However, the computation of the laser ranging station's coordinates on the basis of data other than those from LAGEOS-1&2 observations is desirable for the following reasons (Lejba and Schillak, 2008):

- it significantly increases the number of observations used for determination of the station's coordinates and EOP;
- it allows results comparison between different combinations;
- it allows the determination of coordinates of the stations that may not routinely range to LAGEOS and Etalon satellites (Govind et al., 2007).

Promising results of the station coordinates determination have been obtained for LEO satellites for short period (Lejba and Schillak, 2008; Lejba et al., 2007). The primary motivation of this work is to determine the effectiveness of the laser ranging observations of STARLETTE in the accurate determination of laser ranging station positions and EOP parameters, and to investigate the contribution of Starlette data in the geodynamic study of station behavior, Geocentre and pole motions for a relatively long period. Thus, the main contribution of this work is the use of measurements taken from STARLETTE satellite and both of LAGEOS satellites in the computation of a laser network over a period of 14 years (from October 1993 to February 2007), according to three solutions of data combination, namely LAGEOS-1 (LA-1), LAGEOS-1&-2 (LA-1&LA-2) and LAGEOS-1& Starlette (LA-1&STAR). The proposed methodology contains three steps:

- orbit restitution of different tracked satellites is performed by the Geodesy by Simultaneous Numerical Integration (*Géodésie par Intégration Numérique Simultanée* [GINS]) software (GRGS, France), based on dynamical approach, see Section 2, where two terrestrial gravity field models were used: Grim5-c1 & Eigen-Grace-03s, in order to ensure a good quality on satellite orbits (Gourine et al., 2008);

- estimation of station coordinate updates and EOP residuals is performed using the MATHEMATICS for Localization and Orbitography (*MATHématiques pour la Localisation et l'Orbitographie* [MATLO]) software (OCA & IGN, France) (Coulot and Berio, 2006), see Sections 3 and 5. This estimation provides weekly time series of station positions and daily time series of EOP. In order to express these parameters in the same reference frame (w.r.t ITRF2005), the transformation parameters were calculated using TRANSFOR software (OCA's program);
- analysis of time series of SLR geodetic products according to different combinations based on:
 - frequency analysis by Frequency Analysis Mapping On Unusual Sampling (FAMOUS) software (Mignard, 2005),
 - noise estimation (type and level noise) by the Allan variance method (Feissel-Vernier et al., 2007), see Section 4. This analysis is a diagnosis tool for the geophysical study of the behaviour of station positions, particularly of vertical components and the motion of the pole and the Geocenter variations. The results of the latter were compared with geodynamical models.

Results of 14 years combined SLR data analysis of different satellites (LAGEOS-1&-2 and Starlette) are presented and discussed in Section 5.

2. Orbital arc determination

Orbit restitution of different satellites (LAGEOS-1, LAGEOS-2 and Starlette) is performed by the GINS software. The dynamical models and the reference frame used are listed in Table 1. The satellites' arcs were calculated using observation data from 13 ILRS stations (Table 2), collected during a period of 14 years, from 2 October 1993 to 24 February 2007.

Positioning quality is directly related to the accuracy of the satellite orbits (in addition to the data accuracy itself). For this reason, high altitude geodetic satellites, such as LAGEOS-1 and LAGEOS-2, are used primarily by geodesists for SLR network computation. Indeed, the orbits of these satellites have the advantage of being less sensitive to remaining uncertainties in the dynamical models than low altitude satellites such as Starlette. In addition, the small size of Starlette compared to its mass gives it a much larger sensitivity to the gravitational attraction than to the surface forces due either to the residual atmosphere at the satellite or to radiation pressure (ILRS web site¹). Since a few years, thanks to new space missions like GRACE (Reigber et al., 2005), the scientific community has

¹ Web site of the International Laser Ranging Service (ILRS): <http://ilrs.gsfc.nasa.gov/>.

Table 1
Dynamical models used for computation.

Tableau 1
Modèles dynamiques utilisés dans les calculs statistiques des résidus d'orbite (en mm).

Model	Description
<i>For Orbit</i>	
Earth's gravity field	GRIM5_C1 (For LAGEOS-1&-2) EIGEN_GRACE03S (for Starlette)
Ocean tides	Fes2002
Atmospheric pressure	ECMWF, http://www.ecmwf.int/
Solar radiation (Flux)	ACSOL2
Atmospheric density	DTM94
Planets	DE403
<i>For Station's position</i>	
Terrestrial reference frame	ITRF2005
Celestial reference frame	ICRF
Atmospheric tides	ECMWF
Oceanic loading	LOAD_FES2002
Solid Earth tides	Model in [McCarthy and Petit, 2004]
Solid Earth pole tide	Model in [McCarthy and Petit, 2004]
<i>For EOP</i>	
Pole	EOPC04
Quasi-diurnal variations	Model in [McCarthy and Petit, 2004]
Precession	Model in [Lieske et al., 1977]
Nutation	Model in [McCarthy, 1996]

Table 2
Statistics of the orbit residuals (in mm).

Tableau 2
Statistiques des résidus d'orbites (en mm).

Satellite	Normal points Number & (%)	Mean residual RMS	Mean residual WRMS
LAGEOS-1	543 969 (32.2)	12.7	9.8
LAGEOS-2	521 734 (30.9)	12.2	8.5
Starlette	621 408 (36.8)	18.3	13.9

RMS: Root Mean Square of orbit residuals; WRMS: Weighted Root Mean Square of orbit residuals.

received an improvement in gravity field models. As a consequence, empirical coefficients can be estimated along the orbit with more consistency than before; their role is to compensate part of unknown non-gravitational forces

(constant and periodic). In fact, an accurate gravity model as Eigen-Grace03s was employed for Starlette orbit computation (Gourine et al., 2008).

The ITRF2005 realization has shown that a scale difference between SLR and VLBI exists and has revealed a bias in scale factor between both solutions of about 1.0 ppb (drift of 0.08 ppb/year) at epoch 2000.0 (Altamimi et al., 2007). The ITRF2005 scale is defined by the VLBI technique. Consequently, it was decided to make available to SLR users an SLR solution extracted from the ITRF2005 and re-scaled back by the aforementioned scale and scale rate (Altamimi, 2006). Consequently, this ITRF rescaled version is considered in all our computations.

Table 3 gives some statistics resulting from computations of different satellite orbits. It can be seen that the WRMS of orbit residuals are at the centimetre level, but with more accuracy for LAGEOS satellite orbits, because they have low sensitivity to gravitational and non-gravitational forces effects. However, Starlette data are slightly dominating the measurements set and the average contribution of normal points per satellite is about 36.8% of all data.

3. Network and EOP computation

The processing of SLR measurements, for geodetic product estimation, comprises two steps. The first deals with the computation of the stations' coordinates and EOP parameters using the MATLO software (Coulot and Berio, 2006). The minimal constraints (Altamimi, 2006) were applied for the resolution of the weekly normal equation systems of the network, which are initially singular due the rank defect corresponding to three rotations, in case of the SLR technique (Altamimi, 2006; Coulot and Berio, 2006). In order to define the datum of the network, we have applied the following values of constraints: ± 1 mm ($3.3 \mu\text{as}$) for rotations (R_x , R_y and R_z) and ± 1 cm for range bias per station and per satellite. The reference frame of the network was defined by 08 ILRS stations as described in Table 2. The results obtained are in terms of time series of EOP residuals and of station coordinate updates, which are considered as individual solutions. Each solution generates its proper terrestrial

Table 3
List of the stations involved in computations.

Tableau 3
Liste des stations prises en compte dans les calculs.

N°	Location name, country	ID number	Orbit computation	Reference frame
1	Komsomolsk-na-Amure, Russia	1868	x	
2	McDonald, USA	7080	x	x
3	Yarragadee, Australia	7090	x	x
4	Greenbelt, USA	7105	x	x
5	Monument Peak, USA	7110	x	x
6	Changchun, China	7237		x
7	Koganei, Japan	7328	x	
8	Zimmerwald, Switzerland	7810	x	x
9	Helwane, Egypt	7831	x	
10	Grasse, France	7835	x	
11	Simosato, Japan	7838	x	
12	Graz, Austria	7839	x	x
13	Herstmonceux, United Kingdom	7840	x	x
14	Mt. Stromlo, Australia	7849	x	

reference frame. In this study, the range biases were obtained from the global solution, which consists in estimating the coordinate updates of stations and the range biases over the whole observations period.

The second step concerns the application of seven parameters of Helmert transformation (three translations, one scale factor and three rotations), obtained from TRANSFOR program (OCA's program), on the weekly solutions of the station coordinate updates and daily EOP. This transformation allows projecting the individual solutions according to a combined and homogeneous terrestrial reference frame (w.r.t. ITRF2005). The results of the processing carried out, illustrated hereafter, are expressed according to parameters of transformation (translations, rotations and scale factor (w.r.t. ITRF2005), variations of pole coordinates (X_p , Y_p) and of Length Of Day (LOD) (w.r.t. EOPC04) and topocentric coordinate updates of laser tracking stations (North component: N , East component: E and Up component: U)).

4. Analysis approach

4.1. Frequency analysis

FAMOUS software, developed by F. Mignard (OCA, France) in the framework of the GAIA project (Mignard, 2005), carries out the frequency analysis of a time signal, with any kind of sampling. Usually time-series derived from observations are not regularly sampled (and even can be very irregularly sampled in the case of Geosciences) and the main feature of this application is to handle this sampling. This program detects the existing periods in the signal and estimates the associated amplitudes and phases. The amplitudes and phases of annual and semi-annual signals are estimated from each series using a non-linear least squares method called the Levenberg-Marquard method. The algorithm of this software decomposes a time-series $y(t)$ as a Poisson series where it determines the frequencies η_k and the coefficients $C_k(t)$ and $S_k(t)$:

$$y(t) = C_0(t) + \sum_k [C_k(t) \cdot \cos(2\pi \cdot \eta_k \cdot t) + S_k(t) \cdot \sin(2\pi \cdot \eta_k \cdot t)] \quad (1)$$

where $C_0(t)$, $C_k(t)$ and $S_k(t)$ are polynomial functions of time t expressed by:

$$C_k(t) = c_0 + c_1 \cdot t + c_2 \cdot t^2 + \dots + c_n \cdot t^n \quad (2)$$

with n a degree of each line k , which is fixed by the user.

The first step of the algorithm consists of removing a polynomial trend from the time-series, adjusted by the least squares method. Then, a first least squares periodogram of the residual series is obtained in a set of frequencies. For each frequency, a constant and coefficients of sines and cosines are adjusted. So, the most powerful spectral line is retained and re-estimated by a non-linear optimisation adjustment to detect the next most significant spectral line. At each step, all frequencies, as well as the trend, are readjusted by the Levenberg-Marquard Method. The last step consists in analysing and

filtering the frequencies to keep only the significant spectral lines, by means of frequency resolution and signal-to-noise ratio (S/N) test. The significance of the detected spectral lines is assessed in the spectral domain by dividing the square root of the amplitude by the median value of the noise computed once the line is removed (Collilieux et al., 2007). We adopt the value of 3.0 for analysing the time-series.

As results, the program gives; in addition to the cosine, sine terms and their standards deviations; the values of frequency η , amplitude A and phase φ , where the signal equation can be expressed by (Mignard, 2005):

$$y(t) = A \cdot \cos(2\pi\eta \cdot t + \varphi) \quad (3)$$

According to the error propagation law, the standard deviations of the amplitude and phase are given as:

$$\sigma_A^2 = \frac{1}{A} (C_k^2 \sigma_C^2 + S_k^2 \sigma_S^2) \quad (4)$$

$$\sigma_\varphi^2 = \frac{1}{A^2} (S_k \sigma_C^2 - C_k \sigma_S^2) \quad (5)$$

with,

C_k , σ_C : Cosine term of k -th frequency and its standard deviation;

S_k , σ_S : Sinus term of k -th frequency and its standard deviation.

4.2. Noise estimation

The Allan variance analysis was developed and is widely used for estimating the frequency stability of atomic clocks (Allan, 1966, 1987). This diagnosis tool was extended to geodetic data (Feissel-Verneir et al., 2007). By definition, the Allan variance of position residuals, for a given time interval, is computed by averaging the position residuals over that interval and computing the variance of differences between adjacent averaged values. This method allows one to characterise the statistical behaviour of time-series, in particular, to identify white noise (spectral density S independent of frequency f), flicker noise (S proportional to $1/f$), and random walk noise (S proportional to $1/f^2$). Let us assume a time-series $(X_j)_{j=1,N}$ regular on a constant interval τ_0 , for a given sampling time τ (with $\tau = M \times \tau_0$), the Allan variance estimation is defined by:

$$\hat{\sigma}_X^2(\tau) = \frac{1}{2(N-2M+1)} \sum_{k=1}^{N-2M} (\bar{X}_{k+M,M} - \bar{X}_{k,M})^2 \quad (6)$$

The Allan variance can be expressed in function of the spectral density S , as:

$$\hat{\sigma}_X^2(\tau) = \tau^{-2} \times 2 \int_0^{+\infty} f^{-2} S_X(f) \frac{\sin^4(\pi f \tau)}{\pi^2} df \quad (7)$$

A convenient and rigorous way to relate the Allan variance of a signal to its error spectrum is the interpretation of the Allan diagram, which gives the changes of the Allan variances for increasing values of τ , in logarithmic scales, corresponding to the following equation:

$$\log [\hat{\sigma}_X^2(\tau)] = \mu \log(\tau) + const \quad (8)$$

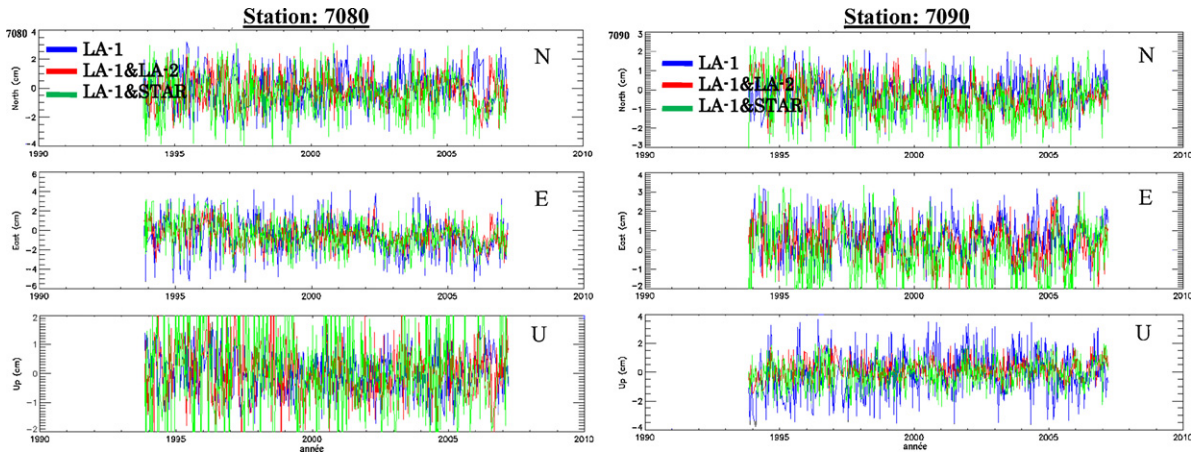


Fig. 1. Topocentric coordinate updates of SLR stations: 7080 and 7090. The series corresponding to the satellites combinations are in red for LA-1, in green for LA-1&2, and in blue for LA-1 & STAR.

Fig. 1. Appoints sur les coordonnées topocentriques des stations SLR : 7080 et 7090. Les séries temporelles correspondant aux combinaisons : LA-1 sont en rouge, LA-1&2 sont en vert, LA-1&STAR sont en bleu.

with μ a slope which takes values -1 , 0 and $+1$ corresponding to white noise, flicker noise and random noise, respectively. In the case where μ takes values between -1 and 0 or 0 and $+1$, it corresponds to a combination of noise types.

The noise type is measured by the slope of the Allan graph, which describes the log-log relationship of the Allan variance of the time series. The noise level is measured by the Allan deviation for a one-year sampling time of the non-linear, non-seasonal position time-series. These estimations are performed under a stationarity assumption (Feissel-Vernier et al., 2007), i.e., the scattering of the data is homogenous in time. Here, the autocorrelation function is used in order to check the stationarity of the time series.

In the context of this study, a white noise signature in the position residuals would point to random errors (Gaussian errors) affecting the measurements, while a flicker noise signature would point to perturbations that may have different origins, such as local tectonics, instrument defects, analysis consistency, etc. (Feissel-Vernier et al., 2007). Concerning the random walk, which is caused by uncorrected jumps in a time-series, it is not found in our analysis.

5. Results and analysis

5.1. Stations coordinate updates

The station position time series are estimated with respect to the ITRF2005 mean position corrected from plate tectonics motion (ITRF2005 velocities), Earth solid tides, pole tide and oceanic loading effects. These time series must consequently show the atmospheric and/or hydrologic loading effects. Fig. 1 gives examples of time series of topocentric coordinate updates (N , E , U) for two stations McDonald (7080) and Yarragadee (7090), according to different solutions of combination. Table 4 exhibits the statistics of results obtained on coordinates updates of

some ILRS stations. The contribution of the Starlette data on the determination of the estimated parameters of these stations is as follows:

- increase of number of solutions compared to those obtained from the LA-1 and LA-1&LA-2 combinations;
- improvement, of a few millimeter, of some stations coordinates quality; for example UP component of station 7090 and East component of station 7105; by adopting the LA-1&STAR solution compared to LA-1 one. However, a degradation of quality on coordinate updates is observed, of about 3 to 5 mm, which is mainly due to a noise induced by the forces effects on the low altitude orbit of Starlette.

The advantage of the time series of station coordinates calculated in a homogeneous reference frame is to enable us to highlight residual signals compared to the a priori signals used in modelling (geophysical signals). In this framework, is carried out a frequency analysis on vertical component series of some stations by FAMOUS software. We have focused on this component because it is important for the geodynamical studies since it holds two-thirds amplitude of signals acting on the station motion (Coulot, 2005).

The results in terms of amplitude and phase of the signal in each UP series of station and according to combination solutions (LA-1, LA-1&LA-2 and LA-1&STAR) are given in Table 5. Annual and semi-annual signals, in vertical time series of stations (7080, 7840, 8834, 7110 and 7839), with amplitudes between 1 to 8 mm can be estimated. Since the effects of ocean loading were considered in the a priori model of orbit restitution, the estimated signals are probably related to residual loading effects as atmospheric and/or hydrologic loading effects, which typically have amplitudes of a few mm.

Fig. 2 gives an example of comparison between the UP periodic signals according to the different combinations

Table 4

Offsets, RMS and number of solutions of the local coordinates of some stations, according to different combinations.

Tableau 4

Appoints, EMQ et nombre de solutions des coordonnées topocentriques de quelques stations, suivant les différentes combinaisons.

Station	Combination	North (cm)		East (cm)		Up (cm)				
7090	LA-1	-0.1	±0.90	527	0.7	±1.02	605	-0.1	±1.52	594
Yarragadee	LA-1&LA-2	-0.3	±0.84	590	0.3	±0.96	602	0.2	±0.69	580
	LA-1&STAR	-0.5	±1.14	599	-0.1	±1.39	600	-0.1	±0.96	587
7105	LA-1	0.1	±1.20	459	-0.4	±1.88	489	-0.1	±0.62	513
Greenbelt	LA-1&LA-2	-0.1	±0.90	521	-0.5	±0.99	531	-0.1	±0.87	528
	LA-1&STAR	-0.1	±1.43	568	-0.2	±1.49	556	0.1	±1.34	561
7403	LA-1	-0.4	±2.68	230	-0.6	±1.60	246	0.6	±2.22	261
Arequipa	LA-1&LA-2	-0.8	±1.41	304	-0.9	±1.46	302	-0.4	±1.81	290
	LA-1&STAR	-1.3	±3.00	368	-1.2	±3.16	369	0.5	±2.81	341
8834	LA-1	-0.2	±1.46	451	0.1	±1.57	461	0.0	±1.30	470
Wetzell	LA-1&LA-2	-0.3	±1.12	489	-0.2	±0.87	468	-0.1	±1.31	488
	LA-1&STAR	0.3	±1.40	507	0.1	±1.36	510	-0.1	±1.68	501
7840	LA-1	-0.4	±1.15	549	0.0	±1.18	536	-0.4	±0.90	576
Herstmonceaux	LA-1&LA-2	-0.4	±0.76	556	-0.4	±0.76	578	-0.3	±0.94	578
	LA-1&STAR	0.0	±1.16	596	-0.1	±1.05	590	-0.1	±1.30	585
7839	LA-1	-0.2	±1.26	512	-0.2	±1.17	497	0.2	±0.96	517
Graz	LA-1&LA-2	-0.1	±0.74	516	-0.2	±0.78	555	0.3	±1.18	576
	LA-1&STAR	0.1	±1.05	547	-0.1	±1.04	549	0.4	±1.36	560

Table 5

Seasonal terms of vertical coordinate (Up component) of some stations, according to different combinations. Amplitude (A in mm) and Phase (φ in degrees).

Tableau 5

Termes saisonniers de la composante verticale (Up) de quelques stations, suivant les différentes combinaisons.

Station	Period	LA-1		LA-1&LA-2		LA-1&STAR	
		A ± σ A	φ ± $\sigma\varphi$	A ± σ A	φ ± $\sigma\varphi$	A ± σ A	φ ± $\sigma\varphi$
7110 Monument Peak	1 yr	1.2 ± 0.6	215.2 ± 30.7	3.7 ± 0.7	241.8 ± 12.5	4.1 ± 0.7	263.9 ± 18.8
7090 Yarragadee	1 yr	6.6 ± 1.3	43.5 ± 11.4	–	–	2.1 ± 0.8	53.4 ± 23.2
	½ yr	–	–	1.4 ± 0.4	177.3 ± 33.7	–	–
7080 McDonald	1 yr	–	–	2.9 ± 0.9	220.9 ± 17.4	3.6 ± 1.3	235.4 ± 21.9
	½ yr	-2.4 ± 0.7	139.9 ± 17.4	–	–	–	–
7105 Greenbelt	1 yr	–	–	2.2 ± 0.8	56.8 ± 22.6	4.2 ± 0.7	88.1 ± 20.4
	½ yr	1.6 ± 0.6	220.8 ± 22.3	–	–	–	–
8834 Wetzell	1 yr	–	–	2.9 ± 0.9	350.5 ± 30.4	4.8 ± 1.1	98.9 ± 23.0
	½ yr	–	–	–	–	4.4 ± 1.5	59.0 ± 22.3

and to the atmospheric loads model (ECMWF series), for 7080 and 7090 laser stations. These stations were chosen for their best quality of observational results and for their larger number of normal points of different satellites. The results revealed that there is coherence between the two signals for each station, with correlation of about 40 to 50%, in the case of the LA1&STAR combination. This explains that the UP variations of the two stations (7080 and 7090) are due to atmospheric loadings. The remains variations are come mainly from noise. It is interesting to indicate which type of noise affects the time series of coordinates in order to make diagnosis about the possible sources of errors in the estimation of these parameters. Table 6

provides the noise level and the noise type of some stations UP components. The white noise is the dominant noise in these series according to the different solutions, while a weak flicker noise combined with white noise is observed in case of LA-1 and LA-1&LA-2 solutions (Fig. 3). In addition, a periodic signal was detected in UP series of 7835 station. According to Table 4, the noise level is of about 3 to 7 mm.

5.2. Transformation parameters

Table 7 summarizes the statistics of the weekly series of Helmert transformation parameters (translation

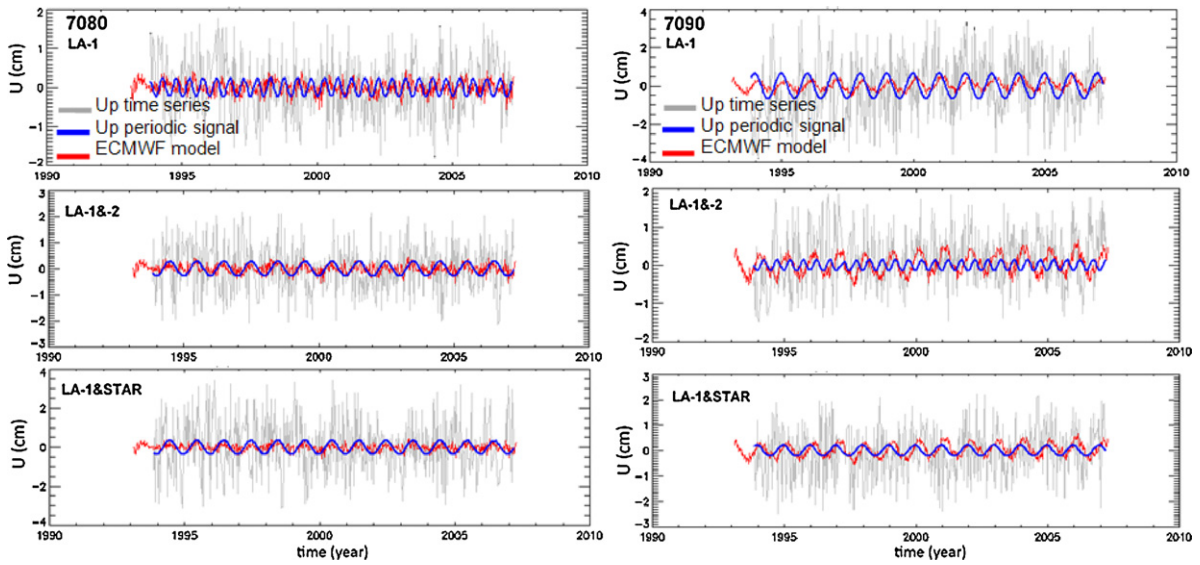


Fig. 2. Comparison between seasonal signals of the Up components and atmospheric loading model (ECMWF) for 7090 and 7080 stations.

Fig. 2. Comparaison entre les signaux saisonniers de la composante verticale Up et les charges atmosphériques (ECMWF), pour les stations 7090 et 7080.

components and scale factor), between different combinations solutions and ITRF2005, and the daily series of pole motion parameters (pole coordinates and LOD).

5.2.1. Geocenter variations

Among the weekly transformation parameters computed between the terrestrial reference frames (TRFs) and the ITRF2005, the translation parameters are of particular importance. Indeed, they evidence the Geocenter variations. This is a topic of crucial importance in the Earth deformation theory as well as in the definition and maintenance of the ITRF.

Fig. 4 illustrates the translation time series according to the different Laser measurement combinations of LAGEOS-1&-2 and Starlette satellites. It can be seen that the solution of the combination (LA-1&STAR) is slightly larger compared to the reference solution (LA-1&LA-2). Indeed, in the case of the LA-1&STAR combination, the dispersion is of about 2.7 cm for TX, 2.8 cm for TY and 2.4 cm for TZ, with average RMS of about ±5 mm. However, in the case of the reference solution, it is only of about 2 cm, 1.9 cm and 1.6 cm, for TX, TY and TZ, respectively, with mean RMS of about ±4 mm (Table 7).

Fig. 5 shows a comparison between translation time series from (LA-1&STAR) and (LA-1&STARw) solutions. The

Table 6

Noise affecting the Up component of some SLR stations, according to different combinations. The noise type, white noise (Wh.) or flicker noise (Fl.) are listed when available, ps. means periodic signal.

Tableau 6

Bruit affectant les signaux de la composante verticale (Up) de quelques stations SLR, suivant les différentes combinaisons. (Wh., Fl., ps) correspondent au bruit blanc, bruit de scintillation et signal périodique, respectivement.

Station	Combinaison	Pente (cm/yr)	Niveau de bruit (cm)	Type de bruit
7080 McDonald	LA-1	-0.6	0.3	Wh. + weak Fl.
	LA-1&-2	-0.7	0.4	Wh. + weak Fl.
	LA-1&STAR	-0.9	0.5	Wh.
7090 Yarragadee	LA-1	-0.7	0.6	Wh. + weak Fl.
	LA-1&-2	-0.6	0.3	Wh. + weak Fl. Wh.
	LA-1&STAR	-0.9	0.4	
7835 Grasse SLR	LA-1	-0.4	0.6	Wh. + Fl. + ps.
	LA-1&-2	-0.5	0.6	Wh. + Fl. + ps.
	LA-1&STAR	-0.7	0.7	Wh. + ps.
7110 Monument Peak	LA-1	-0.5	0.3	Wh. + Fl.
	LA-1&-2	-0.6	0.3	Wh. + Fl.
	LA-1&STAR	-0.9	0.4	Wh.

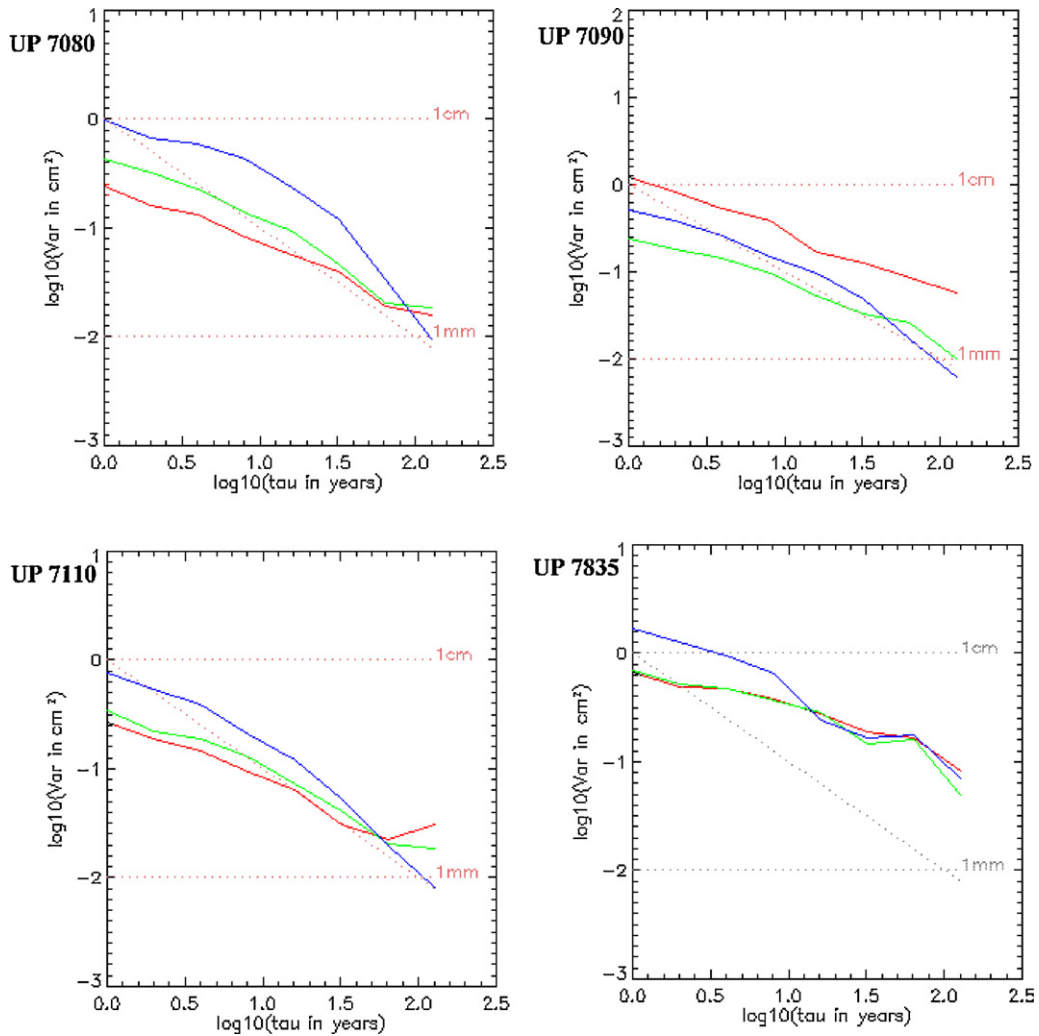


Fig. 3. Allan variance graph of Up component updates of stations 7080, 7090, 7835 and 7110. The series corresponding to the satellites combinations are in red for LA-1, in green for LA-1&-2, and in blue for LA-1 & STAR.

Fig. 3. Graphe de la variance d'Allan de la composante verticale Up des stations 7080, 7090, 7835 et 7110. Les séries temporelles correspondant aux combinaisons : LA-1 sont en rouge, LA-1&-2 sont en vert, LA-1&STAR sont en bleu.

Table 7

Statistics of transformation parameters (translations TX, TY, TZ; scale factor D) and pole parameters (pole residuals coordinates X_p , Y_p and Length of Day LOD) according to different combinations. The values for each parameter are the minimum, maximum, average and WRMS.

Tableau 7

Statistiques des paramètres de transformation (translations : TX, TY, TZ ; facteur d'échelle : D) et des paramètres du pôle (coordonnées résiduelles du pôle X_p , Y_p et longueur du jour LOD) suivant les différentes combinaisons. Les valeurs de chaque paramètre représentent le minimum, le maximum, la moyenne et l'écart-type pondéré.

Solution	TX (cm)		TY (cm)		TZ (cm)		D (ppb)		X_p (mas)		Y_p (mas)		LOD (ms)	
LA-1	-0.93	1.19	-1.19	1.19	-0.90	1.12	-2.40	1.03	-0.66	0.80	-0.74	0.80	-0.15	0.16
	0.12 ± 0.49		-0.27 ± 0.48		0.11 ± 0.46		-0.66 ± 0.69		0.07 ± 0.26		-0.01 ± 0.22		0.00 ± 0.03	
LA-1&LA-2	-0.92	1.00	-0.85	1.00	-0.79	0.78	-1.87	0.76	-0.50	0.61	-0.52	0.61	-0.11	0.11
	0.03 ± 0.39		-0.15 ± 0.35		0.00 ± 0.37		-0.59 ± 0.56		0.05 ± 0.14		-0.02 ± 0.13		0.00 ± 0.01	
LA-1 & STAR	-1.04	1.65	-1.22	1.65	-1.22	1.17	-2.18	1.80	-0.65	0.92	-0.72	0.92	-0.16	0.17
	0.30 ± 0.47		-0.15 ± 0.46		-0.04 ± 0.47		-0.26 ± 0.75		0.14 ± 0.23		0.02 ± 0.20		0.00 ± 0.02	
LA-1 & STARw	-0.85	1.68	-1.39	1.68	-1.08	1.51	-5.10	1.09	-0.64	0.83	-0.65	0.83	-0.15	0.15
	0.39 ± 0.50		-0.10 ± 0.50		0.23 ± 0.49		-2.03 ± 0.78		0.10 ± 0.15		0.05 ± 0.15		0.00 ± 0.02	

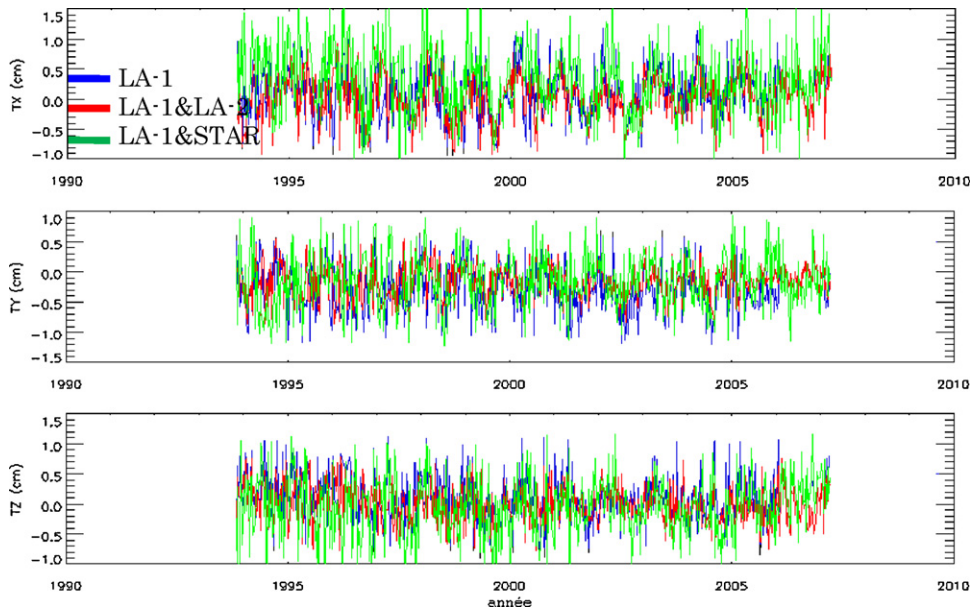


Fig. 4. Time series of the Geocenter variations components (TX, TY, TZ).

Fig. 4. Séries temporelles des composantes des variations du géocentre (TX, TY, TZ).

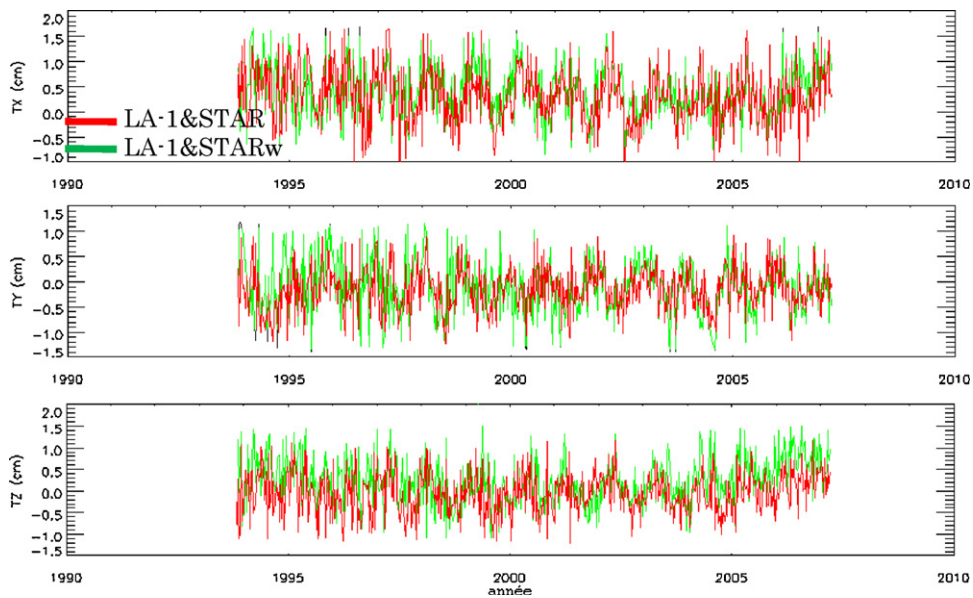


Fig. 5. Comparison of the Geocenter variations components between LA-1&STAR and LA-1&STARw solutions.

Fig. 5. Comparaison des composantes des variations du géocentre entre les solutions LA-1&STAR et LA-1&STARw.

latter is obtained by weighting the Starlette observations taking into account the corresponding standard deviations which are twice larger than those of LAGEOS performing the degree of freedom method (Coulot, 2005 for more details), in order to evaluate the effect of weighting on the results. It can be noted that the results are considerably equivalent for the parameters (TX and TY), and with a less degree, for the TZ component.

The Geocenter variations are mainly due to the redistribution of masses in atmosphere, in oceans and

also in hydrological reservoirs. In general, they present two principal periodic components: annual and semi-annual terms. Table 8 displays the values of amplitudes and phases of annual and semi-annual terms of our solutions, ILRS solution (Collilieux et al., 2009), and two geophysical models of Chen et al. (1999) and Dong et al. (1997), computed taking into account atmospheric pressure data, ocean tides and surface water data. The comparison between LA-1&STAR results and those of the other authors revealed agreements at millimeter level for the

Table 8

Comparison of seasonal Geocenter components (TX, TY, TZ) and scale factor (D) variations of combinations solutions with ILRS estimates (Collilieux et al., 2009) and geophysical models of Chen et al. (1999) and Dong et al. (1997). A and φ are, respectively, the amplitude in mm, and the phase in degrees.

Tableau 8

Comparaison entre les termes saisonniers des composantes du Géocentre (TX, TY, TZ) et des variations du facteur d'échelle (D) des différentes combinaisons avec les estimations de l'ILRS (Collilieux et al., 2009) et les modèles géophysiques de Chen et al. (1999) et Dong et al. (1997). A et φ sont, respectivement, l'amplitude en mm et la phase en degrés.

Parameter	Combinations solutions				ILRS	Chen et al. (1999)	Dong et al. (1997)
	LA-1&STARw	LA-1&-2	LA-1&STAR	LA-			
TX A 1 yr	2.3 ± 0.3	2.4 ± 0.3	3.3 ± 0.4	2.4 ± 0.4	2.7 ± 0.3	2,4	4,2
TX φ 1 yr	279.5 ± 16.7	280.4 ± 13.7	300.5 ± 11.9	296.4 ± 15.7	45 ± 6	244	224
TX A ½ yr		0.7 ± 0.2		0.8 ± 0.3	–	0,7	0,8
TX φ ½ yr		277.6 ± 42.9		96.2 ± 50.6		1	210
TY A 1 yr	1.5 ± 0.2	1.1 ± 0.3	2.0 ± 0.2	3.1 ± 0.6	3.8 ± 0.2	2,0	3,2
TY φ 1 yr	88.9 ± 25.0	65.1 ± 22.2	0.1 ± 20.4	51.9 ± 10.9	327 ± 4	270	339
TY A ½ yr				0.9 ± 0.4	–	0,9	0,4
TY φ ½ yr				337.7 ± 43.8		41	41
TZ A 1 yr	1.3 ± 0.5	1.3 ± 0.3	2.3 ± 0.4	2.2 ± 0.3	3.6 ± 0.4	4,1	3,5
TZ φ 1 yr	322.9 ± 23.3	332.1 ± 17.6	290.9 ± 16.8	261.4 ± 21.0	4 ± 7	228	235
TZ A ½ yr					–	0,5	1,1
TZ φ ½ yr						58	133
D A 1 yr	0.7 ± 0.3	0.6 ± 0.2	1.0 ± 0.3	2.0 ± 0.5	1.7 ± 0.2	–	–
D φ 1 yr	201.7 ± 35.8	96.1 ± 35.8	189.4 ± 29.6	29.0 ± 17.6	144 ± 8		
D A ½ yr	0.7 ± 0.3		0.9 ± 0.3		0.7 ± 0.2	–	–
D φ ½ yr	20.7 ± 33.2		257.9 ± 32.7		3 ± 17		

amplitudes. Better agreements for annual and semi-annual terms, of LA-1&STARw compared to ILRS solution and both geophysical models in the TX and TY components.

For phases, the agreements are less convincing. This is probably due to the choice of reference frame and physical models used in the computations (Coulot and Berio, 2006). The spectral behavior of time series of Geocenter motion, described by the method of the Allan variance, is shown in Fig. 6a. After removing the trend (estimated by linear regression) and the periodic components (annual and semi-annual terms), we applied the Allan variance on the resulting Geocenter motion time series. The dominant noise type in these series is white noise. However, the noise affecting the three Geocenter components of LA-1&STAR solution is slightly important, being about 2 mm. The solution (LA-1&LA-2) remains the least disturbed with a noise level of about 1 mm. On the other hand, Table 9 and Fig. 6b show that the weighting of Starlette measurements

affected only the TZ component where the type of noise is a flicker noise, with the same order of 2 mm.

5.2.2. Scale factor variations

Scale factor variations of the reference frame are affected by errors of the stations' vertical component determination (Coulot, 2005). Thus, the range biases and errors on the radial components due to residual orbital errors, which limit the accuracy of the vertical components, affect the scale factor variations. On the other hand, the network effect (Collilieux and Altamimi, 2008) is another factor that may also affect the scale factor. Fig. 7 shows the time series of the scale factor variations, corresponding to different combinations.

From Table 7, the dispersion of the (LA-1&STAR) series is of the order of 4.0 ppb with an RMS of ± 0.56 ppb (or 24 ± 5 mm). In the case of LAGEOS solutions, it is about of 2.7 ppb with RMS of ± 0.75 ppb (or 16 ± 3 mm). This shows

Table 9

Noise of the translations and scale factor time series. Slope of the Allan variance log-log graph designs the noise type and NL is the noise level.

Tableau 9

Bruit des séries temporelles des paramètres de transformation et du facteur d'échelle. La pente du graphe log-log de la variance d'Allan désigne le type du bruit et NL est le niveau de bruit.

Solution	TX (cm)		TY (cm)		TZ (cm)		D (ppb)	
	Slope	NL	Slope	NL	Slope	NL	Slope	NL
LA-1	–0.9	0.16 ± 0.01	–0.8	0.16 ± 0.01	–0.7	0.16 ± 0.01	–0.6	0.28 ± 0.02
LA-1&LA-2	–0.7	0.14 ± 0.01	–0.7	0.12 ± 0.004	–0.9	0.12 ± 0.01	–0.6	0.22 ± 0.01
LA-1 &STAR	–0.7	0.19 ± 0.02	–0.8	0.17 ± 0.01	–0.7	0.19 ± 0.01	–0.8	0.32 ± 0.04
LA-1 &STARw	–0.8	0.19 ± 0.01	–0.8	0.19 ± 0.01	–0.5	0.22 ± 0.01	–0.8	0.46 ± 0.08

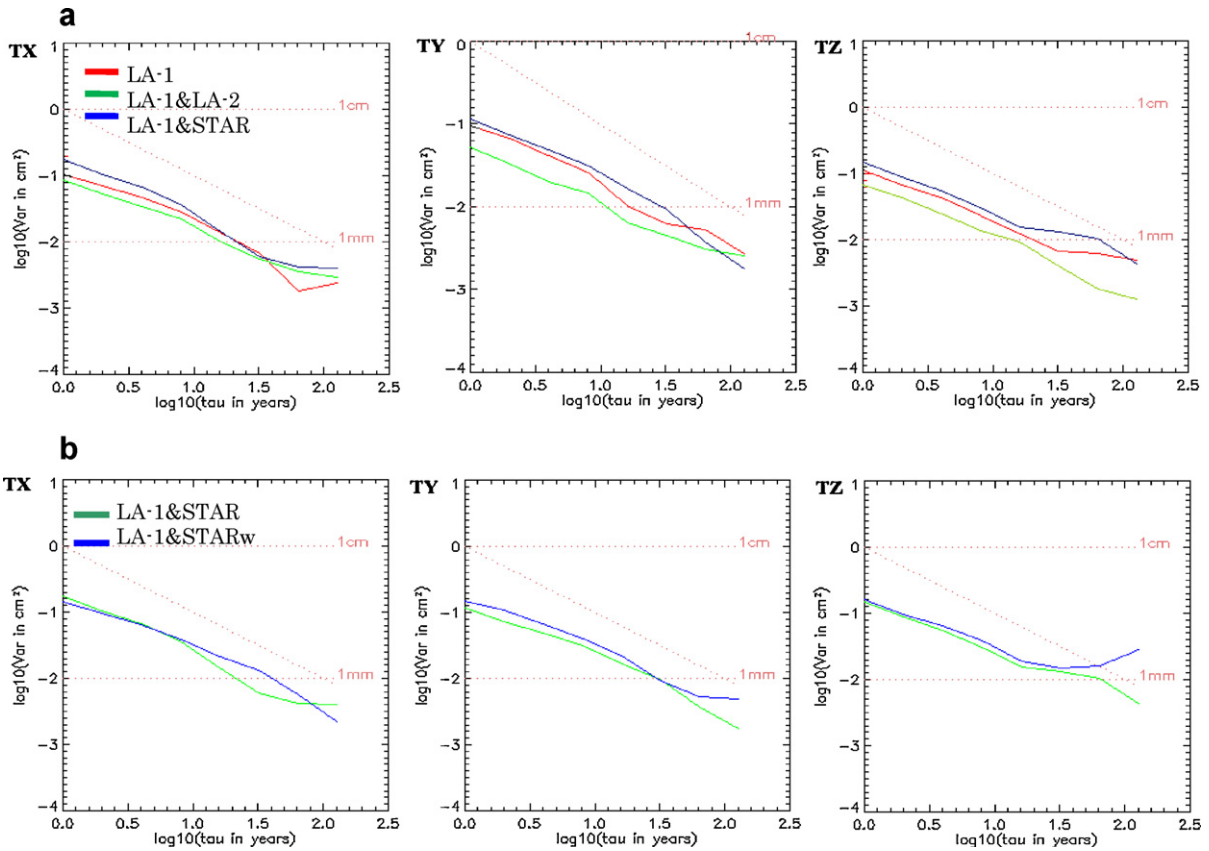


Fig. 6. Allan variance of Geocenter variation components according to: a: all combination solutions (LA-1, LA-1&LA-2 and LA-1&STAR); b: solutions (LA-1&STAR and LA-1&STARw).

Fig. 6. Variance d’Allan des composantes du Géocentre suivant : a : les solutions (LA-1, LA-1&LA-2 et LA-1&STAR) ; b : les solutions (LA-1&STAR et LA-1&STARw).

that Starlette measurements are noisier than LAGEOS ones. Fig. 7b and Table 7 show a shift in magnitude of about 1.8 ppb (or 11 mm) between both time series of LA-1&STAR combinations (weighted and un-weighted measurements of Starlette).

Table 8 provides the values of annual signals and/or semi-annual (amplitudes and phases) of the scale factor.

LA-1&STAR solution contains both periodic components with an amplitude of about 0.17 ppb/yr and 0.15 ppb/06 months (1 mm/yr and 0.9 mm/06 months; slightly higher values compared to those of LAGEOS solutions but with the same RMS). However, the annual amplitude of the LA-1&STARw solution, which is approximately twice larger than LA-1&STAR one, agrees well with ILRS amplitude.

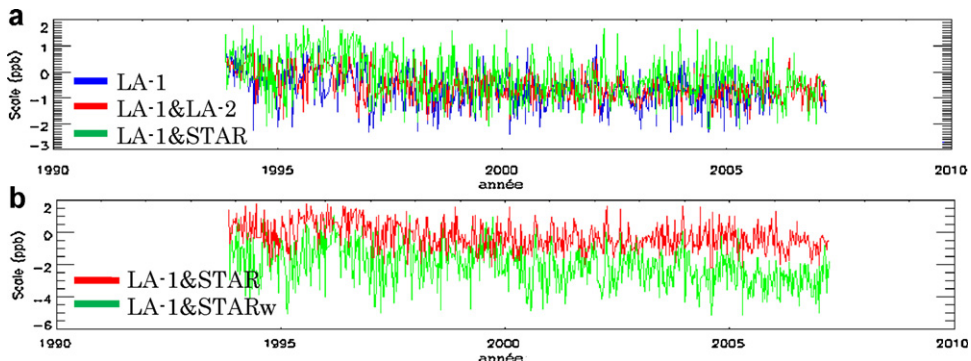


Fig. 7. Time series of scale factor according to: a: different combination solutions (LA-1, LA-1&LA-2 et LA-1&STAR); b: solutions from un-weighted and weighted Starlette measurements (LA-1&STAR and LA-1&STARw).

Fig. 7. Séries temporelles du facteur d’échelle suivant : a : les solutions des différentes combinaisons (LA-1, LA-1&LA-2 et LA-1&STAR) ; b : les solutions (LA-1&STAR et LA-1&STARw).

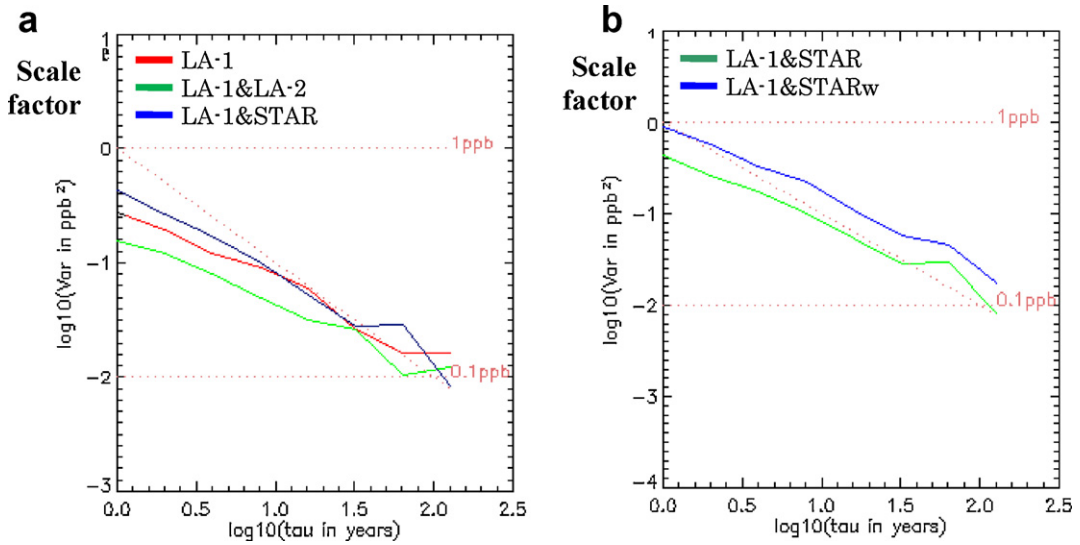


Fig. 8. Allan variance of Scale factor according to: a: all combination solutions (LA-1, LA-1&LA-2 and LA-1&STAR); b: solutions (LA-1&STAR and LA-1&STARw).

Fig. 8. Variance d’Allan des séries temporelles du facteur d’échelle suivant : a : les solutions (LA-1, LA-1&-2 et LA-1&STAR) ; b : les solutions (LA-1&STAR et LA-1&STARw).

Fig. 8 shows the graph of the Allan variance of time series of the scale factor. It can be seen that the dominant noise for combinations using measurements of Starlette is a white noise of about 2 to 3 mm level. For LAGEOS solutions, one notices, in addition to white noise, the presence of flicker noise with a level of 1 to 2 mm (Table 9).

5.3. EOP parameters residuals

Fig. 9 presents the time series residuals of the pole coordinates (X_p , Y_p), and of the LOD. These times series were processed, for different solutions, with respect to the standard solution EOPC04 of IERS, and expressed according to a coherent reference frame with ITRF2005. From Table 2,

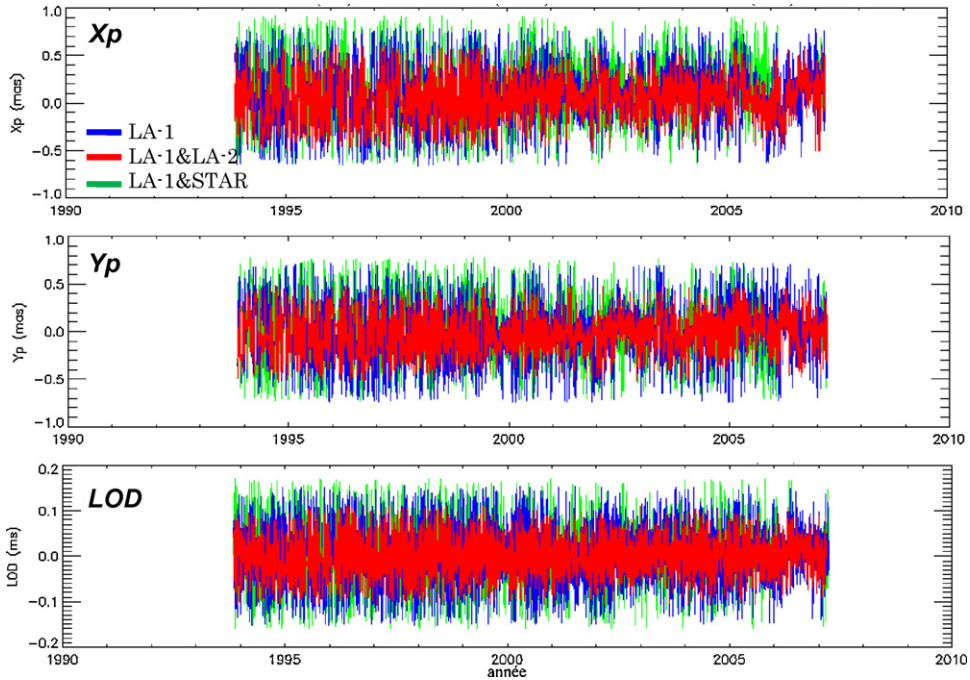


Fig. 9. Time series of pole motion parameters (X_p , Y_p , LOD).

Fig. 9. Séries temporelles des paramètres du pôle (X_p , Y_p et LOD).

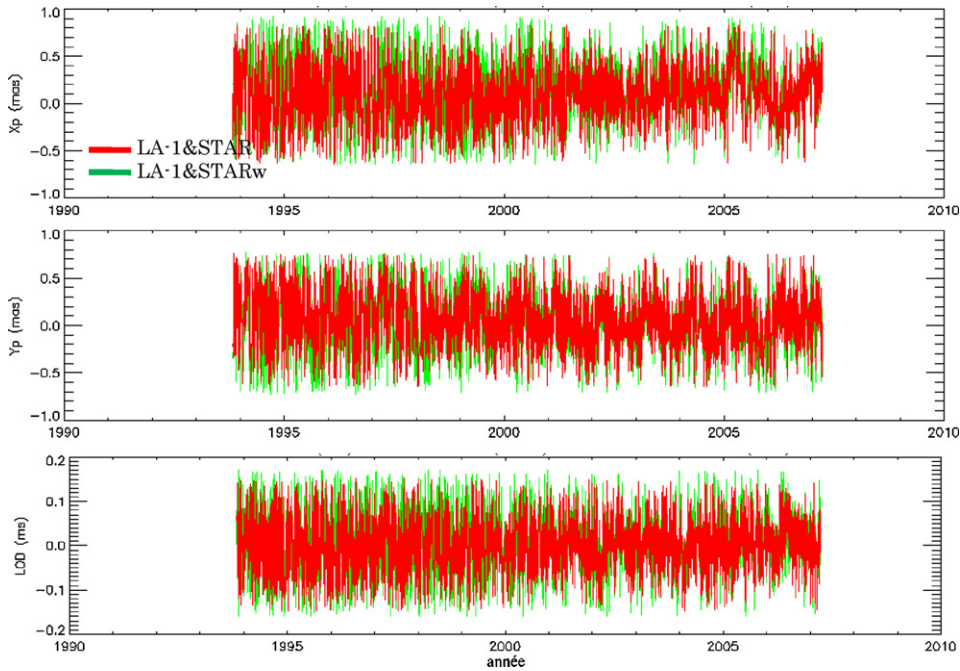


Fig. 10. Time series of pole motion parameters (X_p , Y_p , LOD) according to LA-1&STAR and LA-1&STARw solutions.
 Fig. 10. Séries temporelles des paramètres du pôle (X_p , Y_p , UT et LOD) suivant les solutions LA-1&STAR et LA-1&STARw.

the standard deviations of the (LA-1&2) solution are, respectively, of about 0.14 mas (~4 mm), and 0.01 ms (~5 mm) for the pole coordinates and time.

According to the LA-1&STAR solution, the RMS are slightly large, in the range of 0.20 to 0.23 mas (or, 6–7 mm) for pole coordinates, and 0.02 ms (or 10 mm) for LOD . In addition, the estimation of pole parameters is satisfactory for the SLR technique and the obtained values are coherent with published values of IERS, which are at a level of 200–300 μ as (Gambis, 2004).

Fig. 10 shows an agreement between both time series of the LA1&STAR solutions, in the case of weighted and unweighted Starlette observations. In fact, in terms of RMS, the two series are at a level of 5 to 6 mm for pole coordinates and of about 10 mm for LOD ; Table 2. The EOP solutions obtained by SLR technique appear to be

inconsistent with EOPC04 at level of 5 to 10 mm (~200 to 300 μ as) (Gambis, 2004).

Table 10 depicts the results of frequency analysis of pole parameters series, using FAMOUS software. The periodic signals are decomposed, with respect to three periods: inter-annual, annual and short periods (from few days to few months < 100 days). The choice of this decomposition is based on the periods of the geophysical phenomena causing the variations in the pole motion. These phenomena are mainly due to the redistribution of masses in the Earth, oceans and atmosphere (Frède, 1999).

The results of different combinations are very close, because the maximum amplitudes of different signals of polar motion do not exceed 74 μ as (or 2.2 mm). As can be observed, the residual effects of geophysical phenomena, mentioned above, on the polar motion, are weak and of

Table 10
 Periodic signals of the pole parameters (X_p , Y_p and LOD).

Tableau 10
 Signaux périodiques des paramètres du pôle (X_p , Y_p et LOD).

Parameter	Period	LA-1	LA-1&LA-2	LA-1&STAR	LA-1&STARw
X_p (μ as)	Inter-annual	56.3	30.1–40.8	36.1–48.3	33.2–36.6
	Annual	–	31.9	46.7	32.6 ^a
	Short period	30.4–34.1	23.6–28.5	34.5–41.3	31.7
Y_p (μ as)	Inter-annual	46.0	–	39.0	33.0
	Annual	39.7	35.0	72.9	74.4
	Short period	31.4–34.0	10.6–22.2	31.3–36.1	28.1–37.2
LOD (μ s)	Inter-annual	6.4	–	6.5	–
	Annual	5.9	6.0	–	7.2
	Short period	5.4–6.0	3.5–4.1	6.1–13.8	5.8–13.7

^a Corresponds to semi-annual term.

Table 11

Noise of pole parameters. Slope of the Allan variance log-log graph designs the noise type and NL is the noise level.

Tableau 11

Bruit des paramètres du pôle. La pente du graphe log-log de la variance d'Allan désigne le type du bruit et NL est le niveau de bruit.

Solution	X_p (μas)		Y_p (μas)		LOD (μs)	
	Slope	NL	Slope	NL	Slope	NL
LA-1	-0.4	140 ± 2	-0.5	130 ± 3	-0.7	26 ± 0.3
LA-1&LA-2	-0.4	110 ± 1	-0.4	90 ± 1	-0.7	19 ± 0.1
LA-1&STAR	-0.5	140 ± 3	-0.4	0.14 ± 2	-0.7	29 ± 0.2
LA-1 &STARw	-0.5	140 ± 3	-0.4	0.13 ± 2	-0.6	27 ± 0.1

about few millimeters. For *LOD*, the variations are induced by the friction of the winds and ocean currents on the solid Earth surface (Frède, 1999). Similarly, variations of this parameter can be decomposed into three terms. The estimated amplitudes of these terms range from about 4 to 6 μs (approximately 2–3 mm) for LAGEOS combinations and are around 7 to 14 μs (or 4–7 mm) for Starlette and LAGEOS-1 combinations. Generally, these values remain very small because they describe the residual signals of the geophysical phenomena.

According to Table 11, all the combinations are characterised by a flicker noise, with levels of about 3 mm and 4 mm in polar motion, 9.5 mm and 14.5 mm in *LOD*, for LA-1&LA-2 and LA-1&Star, respectively.

6. Conclusion

In this study, we analysed the different SLR data combinations, namely LA-1, LA-1&LA-2 and LA-1&STAR, in order to study the contribution of Starlette laser measurements in the determination of the geodetic products. An average arc RMS of about 1–2 cm has been obtained for LAGEOS-1&2 and Starlette satellites. The stations positioning accuracy according to the local geodetic coordinates (Northing, Easting, Up) is at centimeter level. Small but significant degradation of RMS of about 3 to 5 mm is observed when adding Starlette data, but also a better capability to determine the annual and semi-annual variations of the UP component and, as a result, very probably a capability to determine the station coordinates if no LAGEOS data were available. The RMS obtained on Geocenter variation components are the same for different combinations of about 4 to 5 mm, and are at level of 0.14 to 0.20 mas (\sim 4–6 mm) on pole coordinates, and 0.01 to 0.02 ms (\sim 5–10 mm) on *LOD*, for EOP, which are in good agreement with the values of IERS.

The proposed analysis methodology was based on: frequency analysis; and noise estimation of the time series of the parameters of interest. The combinations of Starlette and LAGEOS-1 data give better results for seasonal signals, which are in good agreements with ILRS terms and geophysical models in the TX and TY components. The type of dominating noise is the white noise, with a level of about 2 mm. The EOP periodic signal is decomposed into inter-annual, annual and short period terms. The flicker noise is the characterizing noise of the EOP time series with a level of about 4 and 15 mm in pole coordinates and *LOD*, respectively, for the LA-1&STAR solutions. On the basis of these results, it is interesting to perform a more global

analysis of different geodetic LEO satellites data in the estimation and interpretation of the geodetic SLR products.

Acknowledgments

Special thanks are given to the GMC team (P. Exertier, P. Berio, D. Feraudy and D. Coulot, etc.) from Observatoire de la Côte d'Azur (OCA), Grasse, France, for their precious technical aid and scientific assistance to achieve this work. The author also thanks S. Kahlouche and B. Ghezali from CTS (Algeria).

References

- Allan, D.W., 1966. Statistics of atomic frequency standards. *Proc. IEEE* 54, 221–231.
- Allan, D.W., 1987. Time and frequency characterisation, estimation, and prediction of precision clocks and oscillators. *IEEE Trans. UFCC* 34, 647–654.
- Altamimi, Z., 2006. Systèmes de référence terrestres : définition, réalisation, application à l'ITRF, état actuel et perspectives. Report of Research, Université Pierre-et-Marie-Curie (Paris 6).
- Altamimi, Z., Collilieux, X., Legrand, J., Garayt, B., Boucher, C., 2007. ITRF2005: a new release of the International Terrestrial Reference Frame based on time series of stations positions and Earth Orientation Parameters. *J. Geophys. Res.* 112, B09401 (doi:10.1029/2007JB004949).
- Chen, J.L., Wilson, C.R., Eanes, R.J., Nerem, R.S., 1999. Geophysical interpretation of observed geocenter variations. *J. Geophys. Res.* 104 (B2), 2683–2690.
- Collilieux X., Altamimi, Z., 2008. Impact of the network effect on the origin and scale: case study of Satellite Laser Ranging, Observing our Changing Earth, Proceedings of the 2007 IAG General Assembly, Perugia, Italy, July 2–13, 2007, International Association of Geodesy Symposia, vol. 133, pp. 31–37, Springer, IAG, doi:10.1007/978-3-540-85426-5-4.
- Collilieux, X., Altamimi, Z., Coulot, D., Ray, J., Sillard, P., 2007. Comparison of very long baseline interferometry, GPS, and satellite laser ranging height residuals from ITRF2005 using spectral and correlation methods. *J. Geophys. Res.* 112, B12403 (doi: 10.1029/2007JB004933).
- Collilieux, X., Altamimi, Z., Ray, J., van Dam, T., Wu, X., 2009. Effect of the satellite laser ranging network distribution on geocenter motion estimation. *J. Geophys. Res.* 114, B04402 (doi:10.1029/2008JB005727).
- Coulot, D., 2005. Télémétrie laser sur satellites et combinaison de techniques géodésiques. Contributions aux systèmes de référence terrestres et applications. PhD thesis, Observatoire de Paris.
- Coulot, D., Berio, P., 2006. Repères de référence terrestres, rotation de la Terre et Télémétrie laser sur satellites. *Géomatique Expert*, N° 50.
- Dong, D., Dickey, J.O., Chao, Y., Cheng, K., 1997. Geocenter variations caused by atmosphere, ocean and surface ground water. *Geophys. Res. Lett.* 24 (15), 1867–1870.
- Feissel-Vernier, M., de Viron, O., Lebail, K., 2007. Stability of VLBI, SLR, DORIS, and GPS positioning. *Earth Planets Space* 59, 475–497.
- Frède, V., 1999. Apport de l'analyse non linéaire à l'étude géophysique de la rotation de la Terre. Thèse, Observatoire de Paris, France.
- Gambis, D., 2004. Monitoring Earth orientation using space-geodetic techniques: state-of-the art and perspective. *J. Geodesy* 78, 295–305.
- Gourine, B., Kahlouche, S., Exertier, P., Berio, Ph., Coulot, D., Bonnefond, P., 2008. Corsica SLR positioning campaigns (2002 an 2005) for satellite altimeter calibration missions. *Marine Geodesy* 31, 103–116 (doi: 10.1080/01490410802053658).

- Govind R., Lemoine F.G., Altimimi Z., LeBail K., Chinn D., 2007. The contribution of Starlette/Stella SLR to terrestrial reference frame definition. GA2A-02, American Geophysical Unions, San Francisco, USA, December 2007.
- Lejba, P., Schillak, S., 2008. Determination of the SLR station coordinates and velocities on the basis of laser observations of low satellites. Proceedings of the 16th International Workshop on Laser Ranging, Poznań – Poland, October 13–17.
- Lejba, P., Schillak, S., Wnuk, E., 2007. Determination of orbits and SLR stations' coordinates on the basis of laser observations of the satellites Starlette and Stella. *Advan. Space Res.* 40 (1), 143–149.
- Mignard, F., 2005. Guide d'utilisation du logiciel FAMOUS. OCA Internal Report, France.
- Reigber, C., Schmidt, R., Flechtner, F., König, R., Meyer, U., 2005. An Earth gravity field model complete to degree and order 150 from GRACE: Eigen-Grace02S. *J. Geodynam.* 39, 1–10.